doi:10.1016/j.jmb.2004.07.052 J. Mol. Biol. (2004) 342, 877–887

JMB

Available online at www.sciencedirect.com

SCIENCE DIRECT®

ELSEVIER

Atomic Force Microscopy Reveals Defects Within Mica Supported Lipid Bilayers Induced by the Amyloidogenic Human Amylin Peptide

J.D. Green[1]†, L. Kreplak[1]†, C. Goldsbury[1], X. Li Blatter[2], M. Stolz[1], G.S. Cooper[3,4], A. Seelig[2], J. Kistler[3] and U. Aebi[1]*

[1]*M.E. Müller Institute for Structural Biology, Biozentrum University of Basel Klingelbergstrasse 70, 4056 Basel, Switzerland*

[2]*Division for Biophysical Chemistry, Biozentrum University of Basel Klingelbergstrasse 70, 4056 Basel, Switzerland*

[3]*School of Biological Sciences Faculty of Science, University of Auckland, Private Bag 92019 Auckland, New Zealand*

[4]*Department of Medicine School of Medicine, University of Auckland, Private Bag 92019 Auckland 1001, New Zealand*

**Corresponding author*

To date, over 20 peptides or proteins have been identified that can form amyloid fibrils in the body and are thought to cause disease. The mechanism by which amyloid peptides cause the cytotoxicity observed and disease is not understood. However, one of the major hypotheses is that amyloid peptides cause membrane perturbation. Hence, we have studied the interaction between lipid bilayers and the 37 amino acid residue polypeptide amylin, which is the primary constituent of the pancreatic amyloid associated with type 2 diabetes. Using a dye release assay we confirmed that the amyloidogenic human amylin peptide causes membrane disruption; however, time-lapse atomic force microscopy revealed that this did not occur by the formation of defined pores. On the contrary, the peptide induced the formation of small defects spreading over the lipid surface. We also found that rat amylin, which has 84% identity with human amylin but cannot form amyloid fibrils, could also induce similar lesions to supported lipid bilayers. The effect, however, for rat amylin but not human amylin, was inhibited under high ionic conditions. These data provide an alternative theory to pore formation, and how amyloid peptides may cause membrane disruption and possibly cytotoxicity.

Keywords: AFM; membrane; amyloid; Langmuir–Blodgett; interaction

Introduction

To date, over 20 peptides or proteins have been identified that can form amyloid fibrils in the body and are thought to cause disease.[1] Three major examples are amyloid-β (Aβ), human amylin (hA), and the prion protein (PrP), involved in Alzheimer's disease, type 2 diabetes and bovine spongiform encephalopathy (BSE), respectively. The amyloid fibrils, which have been described as being several μm long and 8–10 nm in diameter with occasional twisting along the fibril axis, are formed by the abnormal polymerization of otherwise soluble proteins.[1] Amyloid fibrils all share common physicochemical and ultrastructural properties, such as cross-β-strand conformation,[1] and specific dye binding activities (for e.g. Congo red and thioflavin-T).

The propensity of amyloid peptides or proteins to form fibrils *in vitro* parallels their cytotoxicity to cultured cells.[2–5] Amylin peptides derived from different species illustrate this point. Human amylin forms amyloid fibrils *in vitro* and is toxic to cultured pancreatic islet β-cells.[6] In contrast, the rat amylin isoform (rA), despite having 84% amino acid sequence identity to hA, does not form fibrils and is not cytotoxic. More recently, researchers have observed that the toxicity of amyloid peptides seems to be related to the aggregation state of the peptide. It appears that it is small oligomeric assembly intermediates rather than the mature fibrils that are cytotoxic.[7–9] This is supported also by two mutations in human α-synuclein, which have been linked to early-onset familial Parkinson's disease. The mutant peptides are cytotoxic *in vitro*

Present address: C. Goldsbury, Max-Planck Unit for Structural Molecular Biology, c/o DESY Buliding 25b, Notkestrasse 85, 22607, Hamburg, Germany.

† J.D.G. & L.K. contributed equally to the work.

Abbreviations used: hA, human amylin; rA, rat amylin; AFM, atomic force microscopy; EM, electron microscopy.

E-mail address of the corresponding author: ueli.aebi@unibas.ch

0022-2836/$ - see front matter

and accumulate oligomers more rapidly or for longer periods of time than the wild-type α-synuclein, whereas the rate of fibril formation is reduced.[10,11]

To date, the mechanism by which amyloid peptides cause cytotoxicity and disease is not well understood. One of the major hypotheses is that amyloid peptides cause membrane perturbation through changes in membrane fluidity, amyloid peptide channel formation, or free radical production and lipid peroxidation.[12–14] They may affect the plasma membrane as well as internal membranes such as the mitochondrial membranes.[14] These mechanisms may also not be mutually exclusive. Recently, there has been a great amount of interest in the channel activity of several amyloid-forming peptides, including Aβ, hA and PrP.[14] This channel activity can be modulated by electrostatic interactions, lipid composition as well as known amyloid inhibitors.[15–18] The ability of amyloid-forming peptides to permeabilise membranes decreases upon their elongation into fibrils.[19]

Amylin is the primary component of the islet amyloid deposits observed in the pancreas of type 2 diabetics.[20] It is a 37 amino acid residue peptide and is produced in the islet β-cells and co-secreted with insulin. It belongs to a family of peptides (amylin, calcitonin, calcitonin-gene-related-peptide and adrenomedullin) sharing to varying extents metabolic functions in the control of nutrient assimilation, storage and disposal.[21–27] Like other amyloid-forming peptides, hA has been observed to permeabilise lipid membranes.[15,17–19,28] The non-amyloidogenic rA peptide, mature hA fibrils and fresh hA mixed with Congo red or rifampicin, however, do not affect lipid bilayers.[15,19] Ion channels produced in planar lipid bilayer conductance experiments upon addition of hA, had a distinct unit conductance but were poorly selective.[15,18] This suggests that the hA-induced transmembrane ion permeability may not be mediated by the formation of channels with a precise molecular structure. Furthermore, the instability and breakage of the planar lipid bilayers cannot be explained by the formation of discrete ion channels.

Using a dye release assay we confirmed that the hA peptide causes membrane disruption. Time-lapse atomic force microscopy (AFM) of mica supported lipid bilayers revealed that this did not occur by the formation of defined pores but instead, the peptide induced small, stable defects spreading over the lipid surface.

Results

Human amylin causes membrane leakage in a vesicle dye release assay

First, we performed a dye release assay in which either hA or rA was added to lipid vesicles filled with the fluorescent dye calcein and the fluorescence signal was monitored until a plateau was reached. Then the complete release of the dye was measured by adding Triton X-100. The results for hA and rA at different concentrations are summarized in Figure 1. For hA, we observed a release equivalent to 70% of the one obtained with Triton X-100 at a peptide concentration of 10 μM, whereas for rA a peptide concentration of 20 μM gave rise to only a ~13% response.

After the addition of Congo red, an inhibitor of fibril formation,[29] the dye release observed for 5 μM hA was decreased to 6.4% (Figure 1). The results presented here were obtained from peptides that were initially reconstituted in HFIP, and then in water, a protocol that dissolves any preformed fibrils.[30] Similar results were also obtained with peptide dissolved directly in water. These results confirm previous observations that hA induces lipid leakage, whereas rA does not,[19] and that Congo red strongly attenuates the membrane leakage caused by hA.[15]

Human amylin causes membrane lesions that can be detected by AFM but not EM

Due to the recent results suggesting that the amyloid peptides cause membrane leakage *via* the formation of 8–12 nm channels within lipid membranes, we aimed to image these structures.[14,18,19,31] To begin with, we imaged the lipid vesicles used in the dye release experiments by electron microscopy (EM) (Figure 2(a)). After incubation of hA, or the rA peptide for 5–20 minutes at a molar ratio of between 1:10 and 1:5 with the lipid vesicles (concentrations which would give a dye release of 30 and 70%, respectively, for hA), no changes in the surface structure of the lipid vesicles could be detected (Figure 2(b) and (c)). With the standard negative staining technique, membrane protein channels with a diameter above 2–3 nm can be readily visualised by transmission electron microscopy (TEM). As no such channels were depicted, this

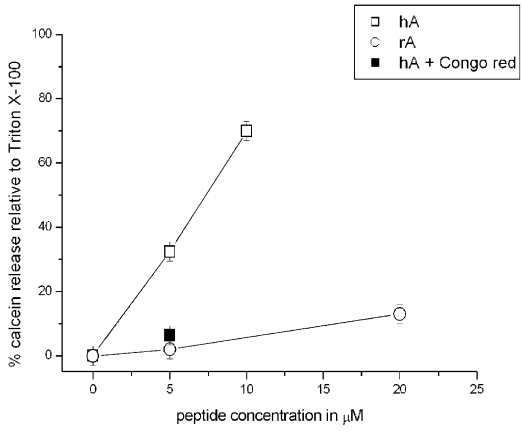

Figure 1. Lipid disruption by hA, hA with a 30-fold molar excess of Congo red (CR), and rA, as judged by the dye release vesicle experiment (5, 10 or 20 μM peptide, 50 μM POPC/POPG (3:1) lipid vesicles, with or without 150 μM Congo red, 10 mM Tris–HCl, 100 mM NaCl, pH 7.4). The lines on the graph are just guidelines for the eye.

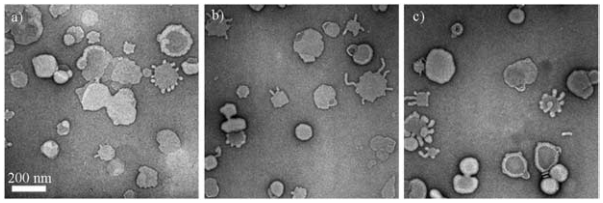

Figure 2. Electron microscopy images of negatively stained (a) calcein-containing large unilamellar lipid vesicles (LUVs), (b) calcein-containing LUVs with hA (10:1 molar ratio) and (c) calcein-containing LUVs with rA (10:1 molar ratio). The LUVs were pre-incubated with the peptide for 20 minutes prior to adsorption on the EM grid.

indicates that either very small protein channels are formed or another mechanism is involved in the membrane permeation.

As an alternative, we employed time-lapse AFM to visualise potential changes that might occur specifically at the membrane surface, an imaging technique that was previously very successful for the observation of the growth of individual hA protofibrils.[32] We applied this technique to image lipid bilayers deposited on a mica surface using the Langmuir–Blodgett technique. Only layers with none (Figure 3(a) and (b): 0 minutes) or very few defects, which revealed the underlying mica support (visible as dark zones in Figure 4(a)–(c): 0 minutes; see arrows), were used for further experiments. Due to the high surface pressure (34–36 mN/m) used, the lipid molecules formed bilayers that were stable and could be repeatedly scanned by AFM for several hours. No rearrangement or healing of defects was observed during imaging, in contrast to what had been previously described for mica-supported lipid bilayers formed after vesicle fusion.[33] It should be noted that a colour coding exists within the images: the darkest

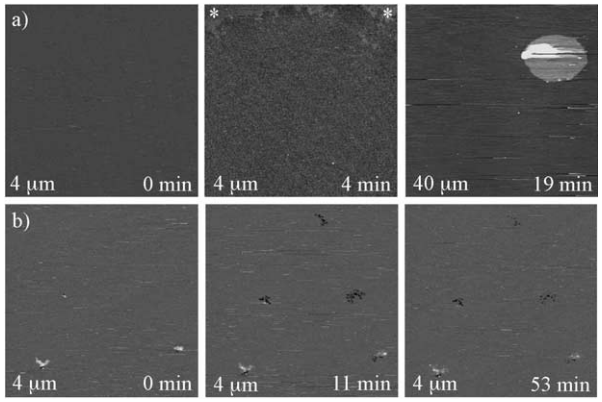

Figure 3. Time-lapse AFM experiments of the effect of (a) 20 μM hA and (b) 20 μM rA on a POPC/POPG (3:1) lipid bilayer (10 mM Tris–HCl, 500 mM NaCl, pH 7.4). The intact lipid bilayer in (a) four minutes is indicated by the asterisk. The scan size and time after the injection of the peptides are displayed in each image.

features are dips or holes within the lipid bilayer, whilst the lightest features represent structures lying above the lipid bilayer. The correct heights/dips of some features are often not resolved due to the large scan size relative to the size of these structures, a finding that has been discussed previously.[34]

In a first set of experiments, we imaged a 4 μm × 4 μm area of the lipid bilayer in 10 mM Tris–HCl, 500 mM NaCl (pH 7.4), to verify that no defects were present within the deposited membrane (Figure 3(a) and (b): 0 minutes). Upon injection of 20 μM hA peptide into the fluid cell, the lipid bilayer was quickly severed (Figure 3(a): four minutes). Within the first image, which took only four minutes to scan from top to bottom, only a small area of the lipid bilayer at the top of the image (which took less than 30 seconds to image) was observed to be intact (Figure 3(a): four minutes; see asterisk). The lipid bilayer in the remainder of the image had a granular appearance. Ten minutes after the injection of hA, the entire lipid bilayer in this area was severed. In a 40 μm × 40 μm area after 19 minutes, only a circular patch of lipid bilayer, with a diameter of approximately 15 μm, was left intact (Figure 3(a): 19 minutes). Notice that the intact bilayer patch was 1.5–2 nm higher than the surrounding severed bilayer. In contrast, rA under similar conditions (i.e. in excess of peptide *versus* lipid) did not make any lesion to the lipid bilayer, except in one of four experiments. In this instance, rA caused the formation of two small defects in the bilayer, which did not increase in size with incubation times up to one hour (Figure 3(b): 11 and 53 minutes).

In a second set of experiments with a 10 mM Tris–HCl (pH 7.4) buffer in the absence of salt, both hA and rA were able to cause lesions in the lipid bilayer (Figure 4(a) and (b)). The lipid bilayer was first imaged without amylin peptides to identify the defects that were present originally in the membrane, revealing the mica surface observed as dark areas in the images (Figure 4(a)–(c): 0 minutes; see arrows). Upon injection of the hA or rA peptide, a halo appeared around these original lesions (Figure 4(a) and (b): see asterisk). In these halo regions the lipid membrane appeared to be 1–1.5 nm lower than the undisturbed lipid bilayer surface. Sometimes a similar decrease in the height of the lipid bilayer also appeared in areas where no initial defect was observed (Figure 4(a) and (b), four minutes; see asterisk). Continuous imaging of the same 4 μm × 4 μm area of the lipid bilayer revealed that the halo regions, which underwent a change in height, grew larger with time (Figure 4(a) and (b)).

The expansion speed of the halos within the lipid bilayer was observed to increase with the peptide concentration from 2.5 μM to 20 μM. This behaviour, however, was modulated by the number of original lipid bilayer defects, thereby increasing the time to affect a given lipid bilayer surface. Because the concentration of peptide and the number of defects seem to affect the expansion speed of the

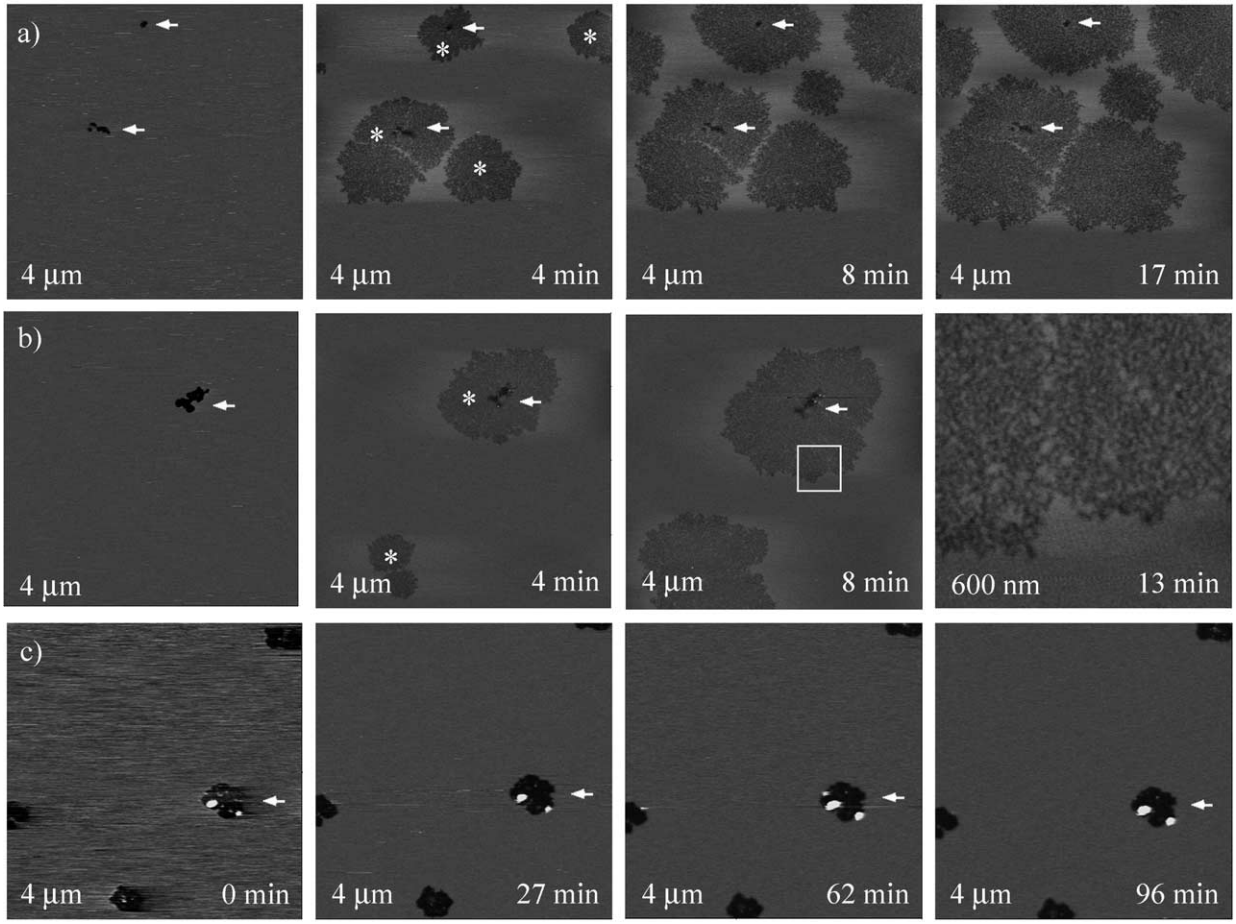

Figure 4. Time-lapse AFM experiments of the effect of (a) 10 μM hA, (b) 10 μM rA and (c) 10 μM hA with 300 μM Congo red, on a POPC/POPG (3:1) lipid bilayer (10 mM Tris–HCl, pH 7.4). The scan size and time after the injection of rA are displayed in each image. Arrows in (a), (b) and (c) indicate the defects present originally in the lipid bilayer. The stars in (a) and (b) indicate lipid disruption following the injection of peptide. A zoom of the membrane disruption framed in (b) eight minutes, is shown in (b) 13 minutes.

halos in an inversely related way, it is difficult to precisely quantify the kinetics of halo formation. As an example, if high peptide concentrations were used (i.e. 10–20 μM), the time for a 4 μm × 4 μm lipid bilayer area to be covered by the halos was between five minutes for a perfect bilayer (Figure 3(a)) and 30 minutes for a lipid coverage of around 80%.

Furthermore, similar to the dye release experiments with the lipid vesicles, the formation of lesions within lipid bilayer by hA could be totally inhibited by the addition of a 30-fold molar excess of Congo red (Figure 4(c)).

Membrane lesions caused by amylin peptides consist of small defects

When the sensitivity of imaging was increased, i.e. by decreasing the scan size, it was observed that the lesions in the lipid bilayer, that had been caused by hA or rA, did not have a uniform aspect (Figure 4(b): 13 minutes). In fact, discrete depressions had formed within the lipid bilayer in these areas (Figure 4(b): 13 minutes). The defects, typically 1.5–2 nm in depth, were not as deep as the original lipid bilayer defects (4–6 nm) where the underlying mica was visible. Quite possibly this was due to the average diameter of the new defects (15–20 nm) being too small for the tip to enter sufficiently deep, and thus to reach the mica surface. The defects were stable over one to two hours and their appearance was distinct from that of pore-like structures typically formed by membrane proteins.

Triton X-100 disrupts lipid bilayers similarly to the human and rat amylin peptides

Because of the observation that the amylin peptides formed multiple small defects in the lipid bilayer rather than pores, we wanted to compare the effect of the amylin peptides with a surfactant known to disrupt lipid bilayers. We therefore investigated the effect of Triton X-100 (0.1 μM) on the lipid bilayer. It was observed that upon injection large 100–500 nm diameter depressions as well as smaller defects were formed (Figure 5: four minutes). Within 13 minutes these large depressions in the lipid bilayer disappeared

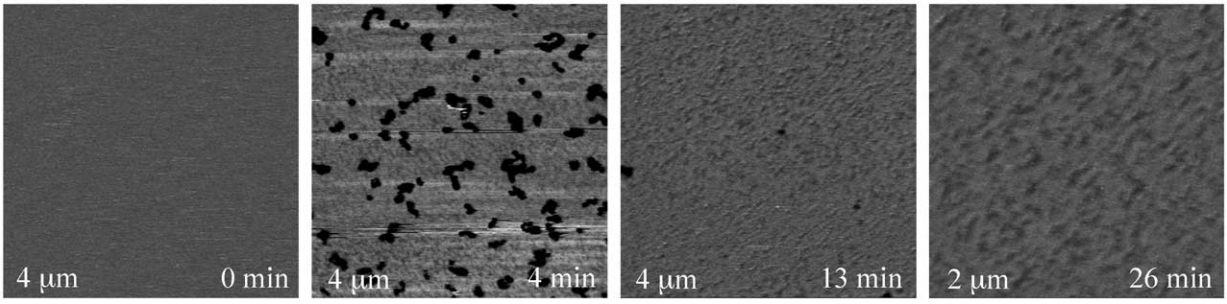

Figure 5. Time-lapse AFM experiments of the effect of Triton X-100 on a POPC/POPG (3:1) lipid bilayer (0.1 μM Triton X-100, 10 mM Tris–HCl, 500 mM NaCl, pH 7.4). The scan size and time after the injection of Triton X-100 are displayed in each image.

and the smaller defects, similar to those caused by the amylin peptides, remained (Figure 5: 13 and 26 minutes). Moreover, at higher peptide concentration (i.e. 0.2 μM) Triton X-100 substantially disrupted the lipid membrane, similar to the results observed with hA as shown in Figure 3(a). Note the difference, though, that Triton X-100 but not the amylin peptides had the ability to promote "membrane healing". It is possible that the lesions caused by the positively charged amylin were stable due to an attractive electrostatic interaction between the peptide and the negatively charged mica surface after defect formation. This attraction of the peptides for the negatively charged mica may also explain why new defects appeared essentially at the periphery of the halos (Figure 4(a) and (b)) whereas for Triton X-100, which has no preferred interaction with mica, the lipid bilayer was uniformly covered with small defects (Figure 5).

Amyloid-β severs lipid bilayers indicating a more generalised mechanism

In order to verify, that the data obtained with hA and rA could be generalised to other amyloidogenic peptides, we performed the same type of AFM experiments using the Aβ peptide. In contrast to hA, Aβ at 20 μM did not form defects in the bilayer upon injection of the peptide into the fluid cell (Figure 6). Instead, after incubation periods of one to two hours, the peptide formed flattened spherical aggregates that increased in size with time (Figure 6: 63, 74 and 118 minutes). These aggregates often formed along the edges of original lipid bilayer defects thereby giving rise to structures that could be interpreted as pore-like if the subsequent images had not been recorded (Figure 6: 180 minutes; see arrows). Although no main lesions occurred within three hours of imaging, when the lipid membrane with the buffer and peptide on top was incubated overnight in a moist chamber and imaged again, small defects with a morphology similar to those observed for hA, were detected (Figure 6: 1920 minutes; see asterisk). The defects are morphologically distinct from the original defects present within the lipid bilayer (see Figure 6: 0 and 1920 minutes; see arrows). These experiments clearly document that Aβ can also affect a lipid bilayer by a mechanism similar to hA, although the kinetics may be different.

Discussion

Amylin has been known for some time to be the principal component of the amyloid deposits that form in the pancreas of patients with type 2 diabetes.[20] Yet the mechanism of hA cytotoxicity has remained poorly understood, although membrane perturbation has been hypothesised.[15,35] In the present work, we have developed a combined fluorescence spectroscopy and microscopy approach to study the interactions of hA and related peptides with lipid bilayers.

A simplified model of cytotoxicity: the membrane lesions hypothesis

Whilst rA and hA have 84% protein sequence identity, their amyloidogenicity and cytotoxicity are very different. Whereas hA readily aggregates into amyloid-like fibrils and is cytotoxic, rA is not amyloidogenic and exhibits no cytotoxicity.[6] Here

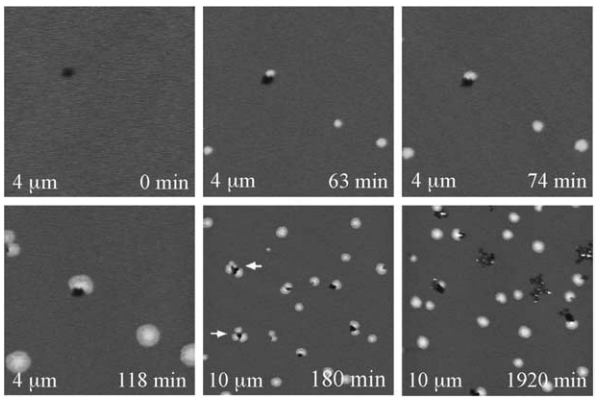

Figure 6. Time-lapse AFM experiments of the effect of Aβ on a POPC/POPG (3:1) lipid bilayer (20 μM Aβ, 10 mM Tris–HCl, pH 7.4). The scan size and time after injection of Aβ are displayed in each image. Arrows at time 180 minutes indicate structures that could be misinterpreted as "pore-like".

we have documented by time-lapse AFM that both hA and rA disrupt lipid bilayers at low ionic strength, but at higher ionic strength, only hA is effective. This indicates that ionic interactions are important for rA to be effective. However, hA's ability to affect the lipid bilayer also under high salt conditions implies that other mechanisms must be involved as well. The difference in hydrophobicity between the hA and rA peptides (-4 *versus* -6.24; hydrophobicity consensus scale[36]) suggests that binding of hA is not only due to electrostatic but also hydrophobic interactions with the lipid bilayer. Hydrophobic interactions have also been shown to be important for the interaction between lipid and PrP.[36,37] If a relatively high salt concentration can inhibit the rA lipid bilayer interactions *in vitro*, we would also expect the effect of rA on lipid membranes to be abolished in the pancreas. We therefore imply that the cell death induced by hA may be due to the direct formation of defects within the cell membrane by a well-balanced contribution of electrostatic and hydrophobic interactions, a task that cannot be performed at higher ionic strength by rA.[2]

To date, the change in structure of the amylin peptides on binding to lipid membranes has not been investigated. However, Aβ, α-synuclein and ApoAI, three other peptides involved in amyloid diseases, have been observed to undergo an increase in and stabilisation of α-helical structure at low concentrations in the presence of negatively charged phospholipid membranes.[38,39] It is also known that proteins often insert into membranes in an α-helical conformation.[40] Interestingly, Aβ's cytotoxicity was eliminated by abolishing the peptide's α-helical conformation by the addition of a proline residue.[41] Furthermore, mutations that have been linked to an early age of onset for Alzheimer's disease have been shown to increase the rate of α-helix formation by the Aβ peptide.[42] Similarly, it may be the ability of hA to increase its α-helical content, prior to the appearance of β-sheet structure and fibrils,[43] that controls its membrane interaction, and simultaneously its cytotoxicity. It may be that rA, at least due in part to its three proline residues, is unable to form a stable α-helical structure which, in turn, is a prerequisite to associate into fibrils.[44–47]

How to explain the membrane lesions caused by amylin and related peptides?

Using time-lapse AFM, we have shown that hA, rA and Aβ peptides can form defects in a mica-supported lipid bilayer. Interestingly, these defects are small, stable and concentrate within regions that can spread over the entire lipid surface. These lipid bilayer lesions are dependent on the concentration of the peptide and on the ionic strength of the buffer. These data imply that in a first instance the various peptides are binding to the lipid bilayer surface taking advantage of attractive ionic interactions. After this first encounter, several mechanisms are plausible, one of the simplest being a carpet-like model similar to that previously suggested for membrane permeation by anti-microbial peptides.[48] In this case, straight amphipathic α-helical peptides initially bind to the surface of the target membrane and cover it or part of it in a carpet-like manner. The target membrane can be permeated only after a threshold deposition has been achieved. According to this model, the peptide molecules rotate after binding, leading to the reorientation of the hydrophobic residues toward the hydrophobic core of the membrane.[48] Finally, micelles are formed which leave the bilayer, resulting in transient defects within the membrane, before total membrane disruption occurs.[48] Most likely, the defects are due to a loss of lipid molecules by the membrane. The other possibility, implying an increase of the membrane packing density by direct insertion of the peptides between lipid molecules, is unlikely, since this is energetically unfavourable. Notice that in this case, the surface covered by the lipid bilayer is supposed to remain constant during the insertion process. However, one should note that in our experimental set-up, the lipid bilayer may still have some room at the border of the hydrophobic ring where it could expand after peptide insertion meaning that the peptide would remain within the bilayer meanwhile decreasing the overall packing density of the peptide–lipid mixture.

In summary, the peptides used here may sever lipid bilayer membranes by causing either a lipid loss similar to that which can also be induced by surfactants such as Triton X-100 or even by high temperature,[49] or an expansion of the lipid bilayer. Both mechanisms could explain most of the experimental findings to date. Considering the lipid loss model, we propose a new interpretation of the earlier patch-clamping and black planar bilayer experiments that assumed a channel-like activity of hA.[18] When the lipid loss occurs *via* micellisation, transient defects are produced.[48] Using the patch-clamping approach, the membrane is free (i.e. not adsorbed to a mica surface like in our AFM experiments) and retains the ability to heal itself after the transient formation of defects, which would lead to apparent channel closures, followed by the formation of new defects again by micellisation somewhere else in the membrane which would constitute new apparent channel openings. The presence of apparently unperturbed vesicles after our dye release experiments (EM data), also argues in favour of such a "mosaic-like opening and closure mechanism". Finally, since the size of the micelles or defects is variable, no well-defined unit conductance should be observed, which is consistent with the published experimental data.[13]

Most importantly, there is still the need for direct quantitative assessment of the lipid fraction solubilised after injection of hA. Such measurement would also rule out the possibility of lipid surface expansion in our AFM experiments.

Studying amyloid peptide–lipid interactions by AFM

Although this is the first microscopy study of the interactions between hA and lipids, several AFM studies have investigated how Aβ and α-synuclein might interact with lipids.[31,50–53] Yip *et al.*, for example, analysed the interactions between Aβ (1–40) or (1–42) and planar lipid bilayers reconstituted from total brain lipid extract using time-lapse AFM.[50–52] In these studies, it was observed that the peptides physically disrupted the bilayers and that this disruption could be decreased with the addition of cholesterol to the membrane. Although fibril formation was often observed to occur within the membrane, it was found not to be necessary for membrane disruption.[52] These reports are consistent with our proposed mechanism, which suggests that lipid loss rather than the formation of discrete protein pores renders the membrane leaky. In contrast, other AFM studies have suggested that pores are formed by amyloid peptides.[31,53] The pore-like structures observed for Aβ protruded by ~1 nm above the lipid bilayer, were 8–12 nm in width, and were built of four or six subunits.[31] Similarly, the appearance of annular protofibrils was reported for α-synuclein thst were 2–3 nm in height and 18–28 nm in width.[53]

A re-evaluation of these latter data may be necessary for the following reasons. In these studies, the Aβ peptide was mixed with the lipid molecules during the vesicle spreading procedure on mica, and underwent a rather harsh treatment which included solubilisation in chloroform, dehydration, resuspension, sonication, and finally heating to 65 °C.[31] Under these conditions it would be energetically favourable for the Aβ peptide to bury its hydrophobic domains within the lipid acyl chains. Although this suggests that pore-like structures might be produced by Aβ oligomers, it does not prove that under physiological conditions the peptide can oligomerise, associate with the lipid and insert into the lipid bilayer. Also, it has not been demonstrated unambiguously that pore formation was peptide-specific. In the AFM experiments imaging α-synuclein annular structures with lipid bilayers, only one oligomer was found on average in each experiment, even though a large area of bilayer was scanned, illustrating that this was a rather rare occurrence.[53] Another explanation for the imaging of these pore-like structures on a lipid bilayer is that the annular protofibrillar Aβ or α-synuclein structures just adsorb on the lipid surface, however without spanning it. Furthermore, the heights of the α-synuclein annular protofibrils above the lipid surface and mica surface were very similar, arguing that these species did not insert into the membrane.[53] It is worth noting that other peptides such as equine lysozyme can form, in solution, annular structures looking like pores or channels.[54]

However, the appearance of pore-like structures as reported by others can be explained by our current results in that Aβ aggregates preferentially around lipid bilayer defects, yielding structures similar to protein pores. Figure 6(e) on its own could be interpreted as pore-like structures being formed from Aβ. The pore could even be thought to span the membrane, as the aggregates formed around the defect that was originally present within the bilayer. It must be acknowledged that the pore-like structures observed with Aβ in our study were approximately 500 nm in size, typically 10–20 times the size for the annular protofibrils. Nevertheless it does illustrate the dangers of only imaging end-points of peptide aggregates forming on a lipid bilayer membrane.

Finally, one should mention that all the AFM studies described in this section, including our present work, were performed with mica-supported lipid bilayers. The mica surface is negatively charged at neutral pH and thus could influence the way slightly positively charged amyloidogenic peptides penetrate lipid bilayers. To circumvent this issue, we, like others, used a mixture of neutral and positively charged lipids that can compete with mica. Using time-lapse AFM we have shown in this study, and for the first-time, that hA and rA still have the tendency to penetrate a mica-supported lipid bilayer, containing negative charges, through defects that are present prior to peptide injection. In this context, it is clear that a detailed model of the cytotoxicity of amyloidogenic peptides cannot be obtained from AFM measurements. However, such experiments reveal interesting trends on peptide–lipid interactions and allow a robust comparison of closely related peptides, as shown here.

Conclusion

The current results demonstrate that time-lapse AFM is a powerful tool not only in the study of amyloid fibrils, but also for understanding the interaction of amyloid peptides with lipid bilayer membranes. The advantage of imaging by AFM is that (i) samples are kept in a physiological buffer environment, and (ii) changes can be monitored in real-time. The ability to observe sample changes rather than only image the end-point was extremely important in the present study on the interaction of amyloid peptides with a lipid bilayer. First, any defects originally present within the lipid bilayer were identified before the addition of peptide. Without this ability, there could have been confusion regarding the aggregates of Aβ on the lipid bilayer and might have led us to a false conclusion regarding the pore-like structures apparently being formed by this peptide. Another advantage of time-lapse AFM is the ability to follow the changes in the sample with time, revealing subtleties between different conditions. For example, we were able to observe that the small defects formed in the lipid bilayer by amylin were stable, and that regions densely covered by these defects were expanding with time. In contrast, after the addition

of Triton X-100 to the lipid bilayer, we observed that the lipid bilayer rearranged itself to yield a final appearance similar to that achieved in the experiments with amylin. The time-lapse AFM experiments on lipid bilayers have shown that the Congo red amyloid dye, known to inhibit fibril elongation, inhibits also the disrupting effect of hA on lipid bilayers. This agrees with our dye release vesicle assay as well as other membrane studies performed by other groups.[15] In an earlier study, we used time-lapse AFM to investigate the effect of Congo red on hA fibril formation and found that hA fibril elongation is inhibited.[55] It may be useful in the future to utilise both time-lapse AFM on a mica surface and on a lipid bilayer to assay the effectiveness of potential inhibitors of amyloid fibril formation.

Materials and Methods

Peptide synthesis and preparation

Lyophilised preparations of synthetic human amylin (KCNTATCATQRLANFLVHSSNNFGAILSSTNVGSNTY) (lot numbers 514905, 538994), rat amylin (KCNTATCATQR LANFLVRSSNNLGPVLPPTNVGSNTY) (lot number 542554) and amyloid-β(1–40) (lot number 518322) were purchased from Bachem (Torrence, CA). Purity was checked by HPLC and MALDI-TOF mass spectrometry. Amylin and Aβ(1–40) stock solutions were prepared by weighing out the appropriate amount of lyophilised peptide and solubilising it in either 1,1,1,3,3,3-hexafluoro-2-isopropanol (HFIP) (Fluka, Switzerland) for one to two days or water for immediate use. The stock solutions in HFIP were prepared in the concentration range of 0.5–3.2 mM as per BCA assay. At the start of each experiment, the HFIP was evaporated off under a nitrogen flow and the peptide dissolved in water. Triton X-100 (Fluka, Switzerland) was prepared as a 1% (w/v) stock solution.

Lipids

1-Palmitoyl-2-oleoyl-*sn*-glycero-3-phosphocholine (POPC) and 1-palmitoyl-2-oleoyl-*sn*-glycero-3-[phospho-rac-(1-glycerol)] (POPG) were bought from Avanti Polar Lipids, Inc. (Alabaster, AL). Lipids were dissolved in chloroform to a concentration of 7 mM and stored at −20 °C.

Dye release assay

The preparation of POPC/POPG (3:1) lipid unilamellar vesicles (LUV) and the dye release experiments were performed as described.[56] Calcein was from Sigma-Aldrich (Steinheim, Gemany). The lipid concentration was determined by quantitative phosphorus analysis.[57] Aliquots of a calcein-containing LUV suspension in 10 mM Tris–HCl, 100 mM NaCl (pH 7.4) buffer (10–20 μl: final lipid concentration 50 μM) were injected into a cuvette containing 2 ml of a stirred peptide solution (5 μM). Calcein release from LUVs, nine minutes after the addition of buffer, peptide or Congo red, was determined fluorometrically by measuring the decrease in self-quenching (excitation at 490 nm, emission at 520 nm) on a Jasco FP 777 spectrofluorometer. The fluorescence intensity corresponding to 100% calcein release was determined by addition of 10 μl of 0.05 g/ml Triton X-100 solution.

Electron microscopy

For negative staining, solutions of calcein-containing LUVs with or without the addition of rA or hA (50 μM peptide, 250–500 μM LUVs, 10 mM Tris–HCl, 100 mM NaCl (pH 7.4), 5–35 minutes pre-incubation) were adsorbed to a glow-discharged carbon-coated collodion film on 400-mesh copper grids. The grids were blotted, washed three times with deionised water, and stained with 2% (w/v) uranyl acetate.[58] Grids were examined in an H-7000 Hitachi transmission electron microscope (Hitachi Ltd., Tokyo, Japan) operated at 100 kV. Images were recorded on Kodak electron image plate film at a nominal magnification of 50,000×.

Mica-supported lipid bilayers

Mica-supported POPC/POPG (3:1) lipid bilayers were produced by Langmuir–Blodgett transfer. A mica plate freshly cleaved in air and immersed in water was lifted through a lipid monolayer spread at the water/air interface, at a surface pressure of 34–36 mN/m, at a speed of 1–2 mm/minute. For finally magnetically mounting the sample in the AFM the mica-supported monolayer was glued onto a circular metal disk (1 cm diameter) using insoluble epoxy glue (Devcon, five minute fast drying epoxy; Glenview, Illinois, USA). The metal disk was lowered through the previously compressed monolayer surface at a speed of 1–2 mm/ minute, forming a stable bilayer. The metal disk was transferred to buffer from the trough, under water. A hydrophobic self-adhesive reinforcement ring with an inner diameter of 6 mm, and an outer diameter of 13 mm (Herma, Germany), covered with silicon sealant on the adhesive side (Dow Corning, USA), was applied to the mica surface of the disk. After one to two minutes, the disk was removed from the buffer, and the buffer droplet was concentrated onto the mica surface, by cleaning off excess silicon using a toothpick. Finally, the mica-supported lipid bilayer protected by the water droplet was kept in a moist chamber at room temperature prior to atomic force microscopy analysis.

At room temperature the POPC/POPG-supported bilayers are in the liquid crystalline state, and 34–36 mN/m is close to the monolayer–bilayer equivalence pressure[59] for which the packing density per lipid molecule is 0.64 nm^2.[60] Then in a supported bilayer which has no defects, the amount of lipid on the mica surface is of the order of 0.15 nmol. Considering that the total volume of buffer used for the AFM experiments is 150 μl, this yields a lipid concentration of roughly 1 μM.

Atomic force microscopy

For time-lapse AFM, mica-supported lipid bilayers covered in 10 mM Tris–HCl (pH 7.4), with 0, 100 or 500 mM NaCl, were imaged in tapping mode to check the initial state of the lipid bilayer. Freshly made amylin or Aβ solutions were injected into the fluid cell to produce a final concentration of 2.5–20 μM. Congo red solutions were freshly prepared in water and filtered three times. Filtered Congo red (Fluka, Switzerland) was added to hA in water, just prior to the addition of buffer and injection into the AFM fluid cell (10 μM hA, 300 μM Congo red, 10 mM Tris–HCl, pH 7.4). For the Triton X-100

experiments, a Triton X-100 solution was injected to produce a final concentration between 50 and 100 ng/ml (approximately 0.1–0.2 μM), in 10 mM Tris–HCl (pH 7.4), 500 mM NaCl. Images were obtained with a Nanoscope IIIa multimode scanning probe workstation (Veeco, Santa Barbara, CA) equipped with a 120 μm scanner (J-scanner) operating in tapping mode using a silicon nitride probe with a nominal spring constant of 0.32 N/m (Veeco). All imaging was performed at scan rates of 1.97 Hz using a cantilever drive frequency of 8–9 kHz. All images were captured as 512×512 pixel scans and were flattened and low-pass filtered. The flattening corresponds to the substraction of a polynomial least-squares fit calculated on each scan line. The low pass filtering is directly performed on the raw image by a weight average over a 3×3 pixels window.

Acknowledgements

We thank Cynthia Tse, Stephanie Bailey and Liselotte Walti for administrative support. This work was supported by grants from the Swiss National Science Foundation (NCCR Nanoscale Science), Novartis Pharma, the M. E. Mueller Foundation of Switzerland, and the Canton Basel-Stadt. G.S.C. is supported by the Foundation for Research Science and Technology, and the Protemix Corporation.

References

1. Sipe, J. D. & Cohen, A. S. (2000). Review: history of the amyloid fibril. *J. Struct. Biol.* **130**, 88–98.
2. DeArmond, S. J., McKinley, M. P., Barry, R. A., Braunfeld, M. B., McColloch, J. R. & Prusiner, S. B. (1985). Identification of prion amyloid filaments in scrapie-infected brain. *Cell*, **41**, 221–235.
3. Forloni, G., Angeretti, N., Chiesa, R., Monzani, E., Salmona, M., Bugiani, O. *et al*. (1993). Neurotoxicity of a prion protein fragment. *Nature*, **362**, 543–546.
4. Lorenzo, A. & Yankner, B. A. (1994). Beta-amyloid neurotoxicity requires fibril formation and is inhibited by congo red. *Proc. Natl Acad. Sci. USA*, **91**, 12243–12247.
5. Schubert, D., Behl, C., Lesley, R., Brack, A., Dargusch, R. Sagara, Y., *et al*. (1995). Amyloid peptides are toxic *via* common oxidative mechanism. *Proc. Natl Acad. Sci. USA*, **92**, 1989–1993.
6. Lorenzo, A., Razzaboni, B., Weir, G. C. & Yankner, B. A. (1994). Pancreatic islet cell toxicity of amylin associated with type-2 diabetes mellitus. *Nature*, **368**, 756–760.
7. Hartley, D. M., Walsh, D. M., Ye, C. P., Diehl, T., Vasquez, S., Vassilev, P. M. *et al*. (1999). Protofibrillar intermediates of amyloid beta-protein induce acute electrophysiological changes and progressive neurotoxicity in cortical neurons. *J. Neurosci.* **19**, 8876–8884.
8. Lambert, M. P., Barlow, A. K., Chromy, B. A., Edwards, C., Freed, R., Liosatos, M. *et al*. (1998). Diffusible, nonfibrillar ligands derived from Abeta 1-42 are potent central nervous system neurotoxins. *Proc. Natl Acad. Sci. USA*, **95**, 6448–6453.
9. Walsh, D. M., Klyubin, I., Fadeeva, J. V., Cullen, W. K., Anwyl, R., Wolfe, M. S. *et al*. (2002). Naturally secreted oligomers of amyloid beta protein potently inhibit hippocampal long-term potentiation *in vivo*. *Nature*, **416**, 535–539.
10. Conway, K. A., Lee, S. J., Rochet, J. C., Ding, T. T., Williamson, R. E. & Lansbury, P. T., Jr (2000). Acceleration of oligomerization, not fibrillization, is a shared property of both alpha-synuclein mutations linked to early-onset Parkinson's disease: implications for pathogenesis and therapy. *Proc. Natl Acad. Sci. USA*, **97**, 571–576.
11. Conway, K. A., Harper, J. D. & Lansbury, P. T., Jr. (2000). Fibrils formed *in vitro* from alpha-synuclein and two mutant forms linked to Parkinson's disease are typical amyloid. *Biochemistry*, **39**, 2552–2563.
12. Kremer, J. J., Pallitto, M. M., Sklansky, D. J. & Murphy, R. M. (2000). Correlation of beta-amyloid aggregate size and hydrophobicity with decreased bilayer fluidity of model membranes. *Biochemistry*, **39**, 10309–10318.
13. Butterfield, D. A., Castegna, A., Lauderback, C. M. & Drake, J. (2002). Evidence that amyloid beta-peptide-induced lipid peroxidation and its sequelae in Alzheimer's disease brain contribute to neuronal death. *Neurobiol. Aging*, **23**, 655–664.
14. Kagan, B. L., Hirakura, Y., Azimov, R., Azimova, R. & Lin, M. C. (2002). The channel hypothesis of Alzheimer's disease: current status. *Peptides*, **23**, 1311–1315.
15. Harroun, T. A., Bradshaw, J. P. & Ashley, R. H. (2001). Inhibitors can arrest the membrane activity of human islet amyloid polypeptide independently of amyloid formation. *FEBS Letters*, **507**, 200–204.
16. Hertel, C., Terzi, E., Hauser, N., Jakob-Rotne, R., Seelig, J. & Kemp, J. A. (1997). Inhibition of the electrostatic interaction between beta-amyloid peptide and membranes prevents beta-amyloid induced toxicity. *Proc. Natl Acad. Sci. USA*, **94**, 9412–9416.
17. Hirakura, Y., Yiu, W. W., Yamamoto, A. & Kagan, B. L. (2000). Amyloid peptide channels: blockade by zinc and inhibition by Congo red (amyloid channel block). *Amyloid*, **7**, 194–199.
18. Mirzabekov, T. A., Lin, M. C. & Kagan, B. L. (1996). Pore formation by the cytotoxic islet amyloid peptide amylin. *J. Biol. Chem.* **271**, 1988–1992.
19. Anguiano, M., Nowak, R. J. & Lansbury, P. T., Jr. (2002). Protofibrillar islet amyloid polypeptide permeabilizes synthetic vesicles by a pore-like mechanism that may be relevant to type II diabetes. *Biochemistry*, **41**, 11338–11343.
20. Cooper, G. J., Willis, A. C., Clark, A., Turner, R. C., Sim, R. B. & Reid, K. B. (1987). Purification and characterization of a peptide from amyloid-rich pancreases of type 2 diabetic patients. *Proc. Natl Acad. Sci. USA*, **84**, 8628–8632.
21. Brain, S. D., Williams, T. J., Tippins, J. R., Morris, H. R. & MacIntyre, I. (1985). Calcitonin gene-related peptide is a potent vasodilator. *Nature*, **313**, 54–56.
22. Castle, A. L., Kuo, C. H., Han, D. H. & Ivy, J. L. (1998). Amylin-mediated inhibition of insulin-stimulated glucose transport in skeletal muscle. *Am. J. Physiol.* **275**, E531–E536.
23. Cooper, G. J. (1994). Amylin compared with calcitonin gene-related peptide: structure. biology, and relevance to metabolic disease. *Endocrinol. Rev.* **15**, 163–201.
24. Cornish, J., Callon, K. E., King, A. R., Cooper, G. J. & Reid, I. R. (1998). Systemic administration of amylin increases bone mass, linear growth, and adiposity in adult male mice. *Am. J. Physiol.* **275**, E694–E699.

25. Hettiarachchi, M., Chalkley, S., Furler, S. M., Choong, Y. S., Heller, M., Cooper, G. J. & Kraegen, E. W. (1997). Rat amylin-(8-37) enhances insulin action and alters lipid metabolism in normal and insulin-resistant rats. *Am. J. Physiol.* **273**, E859–E867.
26. Leighton, B. & Cooper, G. J. (1988). Pancreatic amylin and calcitonin gene-related peptide cause resistance to insulin in skeletal muscle *in vitro*. *Nature*, **335**, 632–635.
27. Young, A. A., Cooper, G. J., Carlo, P., Rink, T. J. & Wang, M. W. (1993). Response to intravenous injections of amylin and glucagon in fasted, fed, and hypoglycemic rats. *Am. J. Physiol.* **264**, E943–E950.
28. Kawahara, M., Kuroda, Y., Arispe, N. & Rojas, E. (2000). Alzheimer's beta-amyloid, human islet amylin, and prion protein fragment evoke intracellular free calcium elevations by a common mechanism in a hypothalamic GnRH neuronal cell line. *J. Biol. Chem.* **275**, 14077–14083.
29. Aitken, J. F., Loomes, K. M., Konarkowska, B. & Cooper, G. J. (2003). Suppression by polycyclic compounds of the conversion of human amylin into soluble amyloid. *Biochem. J.* **374**, 779–784.
30. Higham, C. E., Jaikaran, E. T., Fraser, P. E., Gross, M. & Clark, A. (2000). Preparation of synthetic human islet amyloid polypeptide (IAPP) in a stable conformation to enable study of conversion to amyloid-like fibrils. *FEBS Letters*, **470**, 55–60.
31. Lin, H., Bhatia, R. & Lal, R. (2001). Amyloid beta protein forms ion channels: implications for Alzheimer's disease pathophysiology. *FASEB J.* **15**, 2433–2444.
32. Goldsbury, C., Kistler, J., Aebi, U., Arvinte, T. & Cooper, G. J. (1999). Watching amyloid fibrils grow by time-lapse atomic force microscopy. *J. Mol. Biol.* **285**, 33–39.
33. Reviakine, I. & Brisson, A. (2000). Formation of supported phospholipid bilayers from unilamellar vesicles investigated by atomic force microscopy. *Langmuir*, **16**, 1806–1815.
34. Heymann, J. B., Moller, C. & Muller, D. J. (2002). Sampling effects influence heights measured with atomic force microscopy. *J. Microsc.* **207**, 43–51.
35. Janson, J., Ashley, R. H., Harrison, D., McIntyre, S. & Butler, P. C. (1999). The mechanism of islet amyloid polypeptide toxicity is membrane disruption by intermediate-sized toxic amyloid particles. *Diabetes*, **48**, 491–498.
36. Eisenberg, D. (1984). Three-dimensional structure of membrane and surface proteins. *Annu. Rev. Biochem.* **53**, 595–623.
37. Sanghera, N. & Pinheiro, T. J. (2002). Binding of prion protein to lipid membranes and implications for prion conversion. *J. Mol. Biol.* **315**, 1241–1256.
38. Terzi, E., Holzemann, G. & Seelig, J. (1997). Interaction of Alzheimer beta-amyloid peptide (1-40) with lipid membranes. *Biochemistry*, **36**, 14845–14852.
39. Davidson, W. S., Jonas, A., Clayton, D. F. & George, J. M. (1998). Stabilization of alpha-synuclein secondary structure upon binding to synthetic membranes. *J. Biol. Chem.* **273**, 9443–9449.
40. Shai, Y. (1999). Mechanism of the binding, insertion and destabilization of phospholipid bilayer membranes by alpha-helical antimicrobial and cell nonselective membrane-lytic peptides. *Biochim. Biophys. Acta*, **1462**, 55–70.
41. Kanski, J., Aksenova, M., Schoneich, C. & Butterfield, D. A. (2002). Substitution of isoleucine-31 by helical-breaking proline abolishes oxidative stress and neurotoxic properties of Alzheimer's amyloid beta-peptide. *Free Radic. Biol. Med.* **32**, 1205–1211.
42. Kirkitadze, M. D., Condron, M. M. & Teplow, D. B. (2001). Identification and characterization of key kinetic intermediates in amyloid beta-protein fibrillogenesis. *J. Mol. Biol.* **312**, 1103–1119.
43. Kayed, R., Bernhagen, J., Greenfield, N., Sweimeh, K., Brunner, H., Voelter, W. & Kapurniotu, A. (1999). Conformational transitions of islet amyloid polypeptide (IAPP) in amyloid formation *in vitro*. *J. Mol. Biol.* **287**, 781–796.
44. Westermark, P., Engstrom, U., Johnson, K. H., Westermark, G. T. & Betsholtz, C. (1990). Islet amyloid polypeptide: pinpointing amino acid residues linked to amyloid fibril formation. *Proc. Natl Acad. Sci. USA*, **87**, 5036–5040.
45. Moriarty, D. F. & Raleigh, D. P. (1999). Effects of sequential proline substitutions on amyloid formation by human amylin 20–29. *Biochemistry*, **38**, 1811–1818.
46. Betsholtz, C., Christmansson, L., Engstrom, U., Rorsman, F., Svensson, V., Johnson, K. H. *et al.* (1989). Sequence divergence in a specific region of islet amyloid polypeptide (IAPP) explains differences in islet amyloid formation between species. *FEBS Letters*, **251**, 261–264.
47. Chou, P. Y. & Fasman, G. D. (1978). Empirical predictions of protein conformation. *Annu. Rev. Biochem.* **47**, 251–276.
48. Oren, Z. & Shai, Y. (1998). Mode of action of linear amphipathic alpha-helical antimicrobial peptides. *Biopolymers*, **47**, 451–463.
49. Fang, Y. & Yang, J. (1997). The growth of bilayer defects and the induction of interdigitated domains in the lipid-loss process of supported phospholipid bilayers. *Biochim. Biophys. Acta*, **1324**, 309–319.
50. Yip, C. M., Darabie, A. A. & McLaurin, J. (2002). Abeta42-peptide assembly on lipid bilayers. *J. Mol. Biol.* **318**, 97–107.
51. Yip, C. M., Elton, E. A., Darabie, A. A., Morrison, M. R. & McLaurin, J. (2001). Cholesterol, a modulator of membrane-associated Abeta fibrillogenesis and neurotoxicity. *J. Mol. Biol.* **311**, 723–734.
52. Yip, C. M. & McLaurin, J. (2001). Amyloid-beta peptide assembly: a critical step in fibrillogenesis and membrane disruption. *Biophys. J.* **80**, 1359–1371.
53. Ding, T. T., Lee, S. J., Rochet, J. C. & Lansbury, P. T., Jr. (2002). Annular alpha-synuclein protofibrils are produced when spherical protofibrils are incubated in solution or bound to brain-derived membranes. *Biochemistry*, **41**, 10209–10217.
54. Malisauskas, M., Zamotin, V., Jass, J., Noppe, W., Dobson, C. M. & Morozova-Roche, L. A. (2003). Amyloid protofilaments from the calcium-binding protein equine lysozyme: formation of ring and linear structures depends on pH and metal ion concentration. *J. Mol. Biol.* **330**, 879–890.
55. Green, J. D., Goldsbury, C., Kistler, J., Cooper, G. S. & Aebi, U. (2004). Human amylin oligomer growth and fibril elongation define two distinct phases in amyloid formation. *J. Biol. Chem.* **279**, 12206–12212.
56. Wieprecht, T., Apostolov, O., Beyermann, M. & Seelig, J. (2000). Interaction of a mitochondrial presequence with lipid membranes: role of helix formation for membrane binding and perturbation. *Biochemistry*, **39**, 15297–15305.
57. Böttcher, C. J. F., Van gent, C. M. & Pries, C. (1961). A rapid and sensitive sub-micro phosphorus determination. *Anal. Chim. Acta*, **24**, 203–204.

58. Bremer, A., Haner, M. & Aebi, U. (1997). Negative staining. In *Cell Biology: A Laboratory Hand Book* (Celis, J. E., ed.), 2nd edit., vol. 3, pp. 277–284, Academic Press, New York.
59. Seelig, A. (1987). Local anesthetics and pressure: a comparison of dibucainebinding to lipid monolayers and bilayers. *Biochim. Biophys. Acta*, **899**, 196–204.
60. Evans, R. W., Williams, M. A. & Tinoco, J. (1987). Surface areas of 1-palmitoyl phosphatidylcholines and their interactions with cholesterol. *Biochem. J.* **245**, 455–462.

Edited by W. Baumeister

(Received 12 March 2004; received in revised form 8 July 2004; accepted 13 July 2004)